Efficient heralding of polarization-entangled photons from type-0 and type-II spontaneous parametric downconversion in periodically poled KTiOPO4

Article *in* Journal of the Optical Society of America B · September 2014

DOI: 10.1364/JOSAB.31.002068

CITATIONS
72

READS
3,051

7 authors, including:

Fabian Steinlechner
Fraunhofer Institute for Applied Optics and Precision Engineering IOF
124 PUBLICATIONS **4,141** CITATIONS
SEE PROFILE

Marta Gilaberte Basset
Fraunhofer Institute for Applied Optics and Precision Engineering IOF
30 PUBLICATIONS **370** CITATIONS
SEE PROFILE

Marc Jofre
Universitat Politècnica de Catalunya
70 PUBLICATIONS **819** CITATIONS
SEE PROFILE

Thomas Scheidl
Austrian Academy of Sciences (OeAW)
66 PUBLICATIONS **7,164** CITATIONS
SEE PROFILE

Efficient heralding of polarization-entangled photons from type-0 and type-II spontaneous parametric downconversion in periodically poled $KTiOPO_4$

Fabian Steinlechner,[1,*] Marta Gilaberte,[1] Marc Jofre,[1] Thomas Scheidl,[2] Juan P. Torres,[1,3] Valerio Pruneri,[1,4] and Rupert Ursin[2]

[1]*ICFO—Institut de Ciencies Fotoniques, 08860 Castelldefels (Barcelona), Spain*
[2]*Institute for Quantum Optics and Quantum Information, Austrian Academy of Sciences, Boltzmanngasse 3, 1090 Wien, Austria*
[3]*Department of Signal Theory and Communications, Polytechnic University of Catalonia, Jordi Girona 1-3, 08034 Barcelona, Spain*
[4]*ICREA—Institució Catalana de Recerca i Estudis Avançats, 08010 Barcelona, Spain*
**Corresponding author: fabian.steinlechner@icfo.eu*

Received May 8, 2014; revised July 2, 2014; accepted July 11, 2014;
posted July 11, 2014 (Doc. ID 209002); published August 7, 2014

Ultrabright sources of entangled photon pairs with high heralding efficiency are an important step in the pursuit of high-bit-rate entanglement-base quantum key distribution, as well as an enabling tool for loss-sensitive quantum optics experiments. Here, we present a robust single-mode fiber-coupled source of polarization-entangled photons around 810 nm with both high brightness and heralding efficiency. Our approach is based on quasi-phase-matched spontaneous parametric downconversion (SPDC) from periodically poled $KTiOPO_4$ in a Sagnac loop configuration. We demonstrate a high degree of two-photon polarization entanglement for single-frequency-pumped type-0 and type-II SPDC, and conduct a conclusive comparison in terms of efficiency and spectral characteristics. In light of applications outside a laboratory environment, we evaluate the feasibility of pumping nonlinear crystals with free-running laser diodes.

OCIS codes: (270.0270) Quantum optics; (190.4975) Parametric processes; (270.5565) Quantum communications.
http://dx.doi.org/10.1364/JOSAB.31.002068

1. INTRODUCTION

Entangled photon pairs are essential for many fundamental quantum optics experiments, as well as a key resource in quantum communication [1] and quantum technologies [2]. Several schemes for the generation of photon pairs have been proposed and demonstrated [3–5], but at present the most widely used method is spontaneous parametric downconversion (SPDC) in nonlinear crystals. Recent developments in the field have led to ultrabright, robust, and compact sources of entangled photons [6–8]. These sources are capable of generating pair rates so high that the main limiting factor to the speed of current quantum cryptography systems based on entanglement is saturation of single-photon avalanche detectors (SPADs), due to high single-photon detection rates. The detectors' timing jitter (t_{jitter}) poses another fundamental limitation for maximal useful pair rates. Once the emitted pair rate (R_0) becomes large compared with the coincidence window ($t_c > t_{\text{jitter}}$), multiple pairs emitted within t_c lead to an increased number of so-called accidental coincidences. Since the coherence time of the photons generated in SPDC is small (<1 ps) compared with the typical size of t_c (>100 ps), these accidental coincidences stem from uncorrelated photon pairs and lead to a decrease in entanglement visibility ($V \lesssim 90\%$, for $R_0 \times t_c \gtrsim 0.1$, and $V \lesssim 99\%$, for $R_0 \times t_c \gtrsim 0.01$) [9,10]. Pair detection rates exceeding 1 Mcps per milliwatt of pump power have been demonstrated [8], such that detection-limited performance is already attained for moderate pump powers. In terms of source design, one strategy to allow higher useful pair rates is to improve the source's heralding efficiency. In an ideal source and detection system, the detection of the idler (signal) photon should herald the presence of its conjugate photon with unit probability. In practice, however, limitations due to detector efficiency, transmission losses, and spatially multimode SPDC emission lead to a large overhead of detected single photons whose partners are never detected, which nonetheless contribute to detector saturation and accidental coincidences. In addition to practical considerations, sources with a high heralding efficiency [10–14] are also of fundamental importance to loop-hole-free test of quantum theory [15–17], device-independent quantum key distribution, and other loss-sensitive experiments. Here, we present a bright, fiber-coupled source of polarization-entangled photons, based on SPDC from a 20-mm-long ppKTP crystal, pumped bidirectionally by a 405-nm laser diode in a Sagnac interferometer [18,19]. In contrast to sources demonstrated previously [6,7,20], we optimize the focus parameters of our source with respect to heralding efficiency, leading to a trade-off with overall source brightness. We additionally demonstrate a high degree of polarization entanglement for photon pairs generated in both degenerate type-II (signal and idler at ~810 nm) and nondegenerate type-0 (signal at ~784 nm, idler at ~839 nm) QPM configurations. Previous

results demonstrated for type-0 and type-II SPDC [6–8,20] were obtained with different optical setups and detection equipment, such that a direct comparison in terms of efficiency can be misleading. Hence, we conduct a conclusive comparison between type-0 and type-II SPDC in ppKTP in terms of spectral characteristics and pair-generation efficiency in the same optical setup. In light of applications in harsh environmental conditions, such as those in space [21–24], we evaluate the suitability of pumping with a free-running (FR) laser diode and analyze the spectral properties of multimode-pumped SPDC.

The realization of a compact, rugged mechanical setup that can sustain strong vibrations and thermal fluctuations will be a vital step toward the implementation of an entangled photon source in space and is the subject of ongoing studies funded by the European Space Agency [25].

2. EFFICIENT PAIR GENERATION IN ppKTP

SPDC in non-centrosymmetric crystals is a second-order nonlinear process that generates paired photons, commonly labeled as signal and idler photons, that can exhibit entanglement in various degrees of freedom. A nonlinear material often used to generate photon pairs, due to its large nonlinearity and good transparency for short pump wavelengths, is potassium titanyl phosphate ($KTiOPO_4$ or KTP [26]). For collinear propagation along the crystallographic x axis, KTP has three nonzero second-order tensor coefficients d_{ijk} [27,28], allowing collinear type-0 ($z_p z_s z_i$), type-I ($z_p y_s y_i$), and type-II ($y_p y_s z_i$) quasi-phase-matching (QPM), by appropriate choice of the poling period [29,30]. These configurations are associated with different effective nonlinearities and wave vectors, and thus, exhibit significant differences in terms of efficiency and spectral characteristics. The largest nonlinear coefficient of KTP is associated with the type-0 process ($d_{zzz} \sim 18.5$ pm/V). The nonlinear coefficients of type-II and type-I SPDC are of similar magnitude, due to Kleinman symmetry ($d_{yyz} \sim 3.9$ pm/V, $d_{zyy} \sim 4.7$ pm/V) [27,28]. In terms of their spectral characteristics, type-0 and type-I SPDC [31,32] show comparable temperature dependence and bandwidths, as both involve copolarized signal and idler photons. This is contrasted by the spectral characteristics of the type-II process, in which the photons generated are polarized orthogonally [33,34]. Since the spectral characteristics of type-I SPDC are comparable to those of type-0 SPDC, but the expected efficiency is significantly lower, we omit type-I SPDC in KTP from our following considerations.

Some of the most efficient entangled photon sources demonstrated to date utilize type-0 [7] and type-II [6] phase matching in ppKTP. However, a direct comparison of these results is difficult, since they were obtained with different optics, detectors, and focus geometries. Hence, we conducted a comparison in terms of spectral characteristics and pair-generation efficiency in the same optical setup.

We experimentally characterized the coincidence count rates and spectra of photon pairs generated in x-cut flux-grown ppKTP crystals pumped by a 405-nm fiber-coupled, single-mode, continuous-wave (cw) laser diode. The poling periods of each nonlinear crystal (as specified by the manufacturer) were $\Lambda_0 = 3.425$ μm for collinear type-0 and $\Lambda_{II} = 10$ μm for collinear type-II SPDC with wavelengths around 810 nm at room temperature. Our two samples were mounted side-by-side at the center of a Sagnac-loop configuration, to allow polarization entanglement (see Section 3). For assessment of efficiency and spectral characteristics, the loop was pumped unidirectionally in the clockwise propagating mode, resulting in a polarization product state. The signal and idler photons were split using a dichroic mirror (for type-0 QPM), or a polarizing beam splitter (PBS) (type-II QPM), and each photon was coupled into one of two single-mode fibers (Nufern HP780).

A. Temperature-Dependent Spectra in ppKTP

In order to assess the temperature tuning characteristics (i.e., their temperature stability) we recorded SPDC spectra at crystal temperatures ranging from 20°C to 50°C, using a single-photon spectrometer with an optical resolution of ~0.1 nm. Figure 1 depicts the normalized spectra observed with a 20-mm ppKTP sample, where a large difference between the type-0 and type-II SPDC bandwidths is clearly visible. Figure 2 depicts the temperature-dependent center wavelengths (cwls) of the signal and idler photons, and the full width at half-maximum (FWHM) bandwidth of the signal photons.

The FWHM bandwidth in cw-pumped collinear SPDC (Fig. 2) is determined by crystal length and the group-velocity

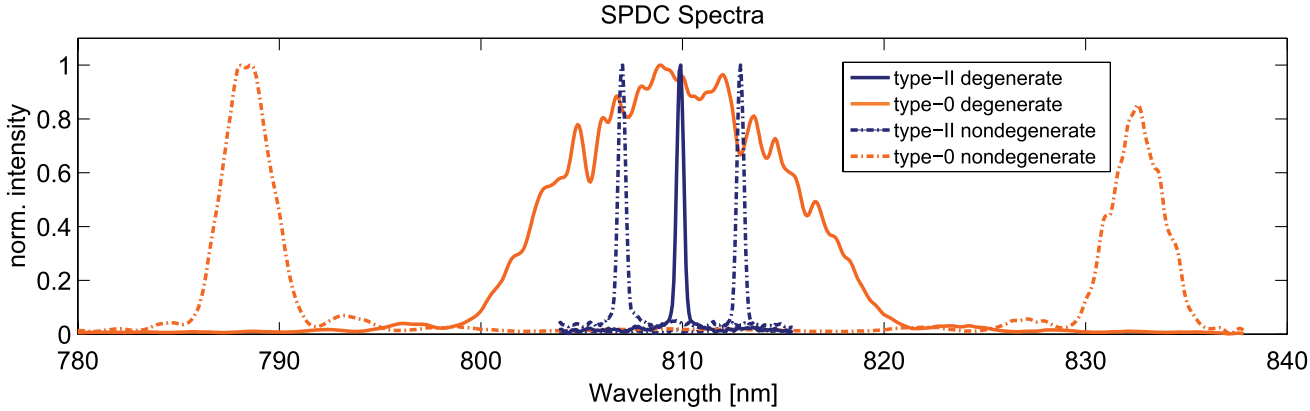

Fig. 1. Normalized spectra of collinear type-0 (orange lines) and type-II (dark blue lines) quasi-phase-matched SPDC in ppKTP: for type-0 SPDC, the FWHM bandwidth for the nondegenerate signal and idler wavelengths (dashed orange line, $T = 29$°C) is smaller than that for wavelength-degenerate QPM (solid orange line, $T = 26.5$°C). The bandwidth of type-II quasi-phase-matched SPDC is smaller for both wavelength degeneracy (solid dark blue line, $T = 35$°C) and nondegeneracy (dashed dark blue line, $T = 20$°C), and is less affected by changes in temperature.

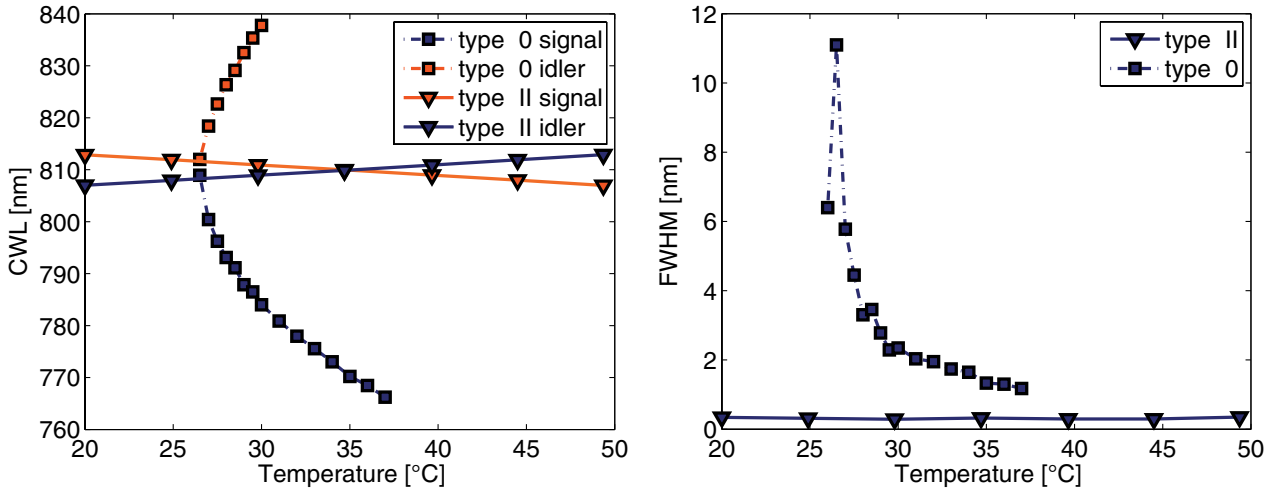

Fig. 2. Spectral characteristics of type-0 and type-II SPDC in 20 mm of ppKTP: the phase-matched cwls (left) of the signal (dark blue solid line) and idler (orange solid line) of type-0 SPDC (squares) show a much stronger temperature dependence than those of type-II SPDC (triangles), and are extended beyond the range of our spectrometer for temperatures above $T \sim 37°C$. Similarly, the FWHM bandwidth (right) of type-0 SPDC shows a stronger temperature dependence than that of the type-II process. (For a relative comparison of bandwidth, see also Table 1.)

mismatch of the signal and idler photons [29,30], and thus, generally decreases with wavelength nondegeneracy ($|\lambda_s - \lambda_i|$). Consequently, a large bandwidth is observed for the copolarized signal and idler photons in type-0 SPDC close to degeneracy ($\lambda_s = \lambda_i = 2\lambda_p$). Although the large bandwidth of the type-0 process close to degeneracy is disadvantageous for typical applications in quantum cryptography, this region can be useful for achieving ultrashort temporal correlations, where a large bandwidth is required [35,36].

For the type-II process, the group velocities of the orthogonally polarized signal and idler already differ significantly at wavelength degeneracy, resulting in a comparatively small bandwidth. Specifically, the observation of nondegenerate type-0 SPDC with the same FWHM bandwidth as the degenerate type-II process would require a wavelength nondegeneracy of ~400 nm for equal lengths of ppKTP crystal [37,38].

The spectral bandwidths obtained experimentally were in good agreement with the values calculated using the Sellmeier material coefficients for KTP [37], for both type-0 and type-II SPDC. The observed temperature dependence of the cwls, however, differed from the calculated behavior, most likely due to the inaccuracy of the refractive index temperature derivatives [38] at the pump wavelength.

B. Pair-Generation Efficiency

The efficiency of a photon-pair source is commonly characterized by its spectral brightness $dR_c/d\lambda/P_0$, that is, the number of pairs generated per milliwatt of pump power (P_0) and per nanometer of generated bandwidth ($\Delta\lambda$), the total pair rate ($R_c \approx (dR_c/d\lambda) \times \Delta\lambda$), and the heralding efficiency ($\eta_{i,(s)} = R_c/R_{s,(i)}$), where $R_{s,(i)}$ is the total number of signal (idler) photons detected. In fiber-coupled SPDC, these parameters are related to the focal parameters of the Gaussian pump and collection modes. Recent theoretical studies suggest that near-unit heralding efficiencies are possible for correctly chosen beam waists of pump and collection modes [39–41]. The spectral brightness is, however, optimized for different focusing conditions, and consequently, a trade-off between rate and heralding must be made [6]. As a general rule, smaller pump waists optimize pair rates, whereas larger waists improve the heralding efficiency, whereby the signal and idler collection waists must be chosen accordingly. A detailed analysis of the optimal focus conditions for Gaussian beams in bulk crystals is beyond the scope of this paper, and can be found in Refs. [39,42].

We chose focus conditions (pump beam waist, $w_p \sim 150$ μm; collection fiber modes, $w_s \sim 80$ μm) that would maximize pair heralding efficiency for a 20-mm-long nonlinear crystal, at the cost of overall brightness, which was a factor of ~0.1 of the peak brightness achievable for smaller waist combinations [39]. The spectral brightness and total pair rates observed for this waist combination as a function of crystal temperature are depicted in Fig. 3. For type-0 SPDC, we observe a spectral brightness that is approximately a factor of 20 higher than that for type-II QPM (Table 1), in good agreement with the relationship between the nonlinear coefficients

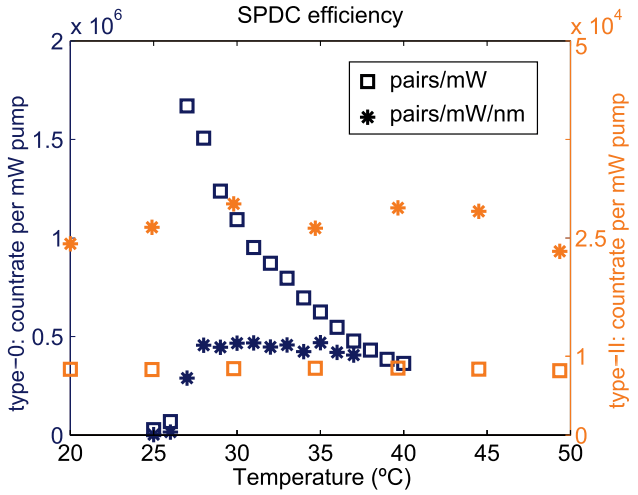

Fig. 3. Pair-generation efficiency in type-0 (dark blue) and type-II (orange) SPDC: spectral brightness (Mcps/mW/nm) remains almost constant over the observed temperature range for both QPM configurations (once the phase-matching condition for type-0 is met at $T = 26.5°C$). Since the total pair rate (Mcps/mW) is proportional to the temperature-dependent bandwidth (Fig. 2), it decreases strongly with temperature for type-0 SPDC.

Table 1. Performance Characteristics of Nondegenerate Type-0 and Degenerate Type-II SPDC in a Unidirectionally Pumped Sagnac Loop

Configuration	λ_s, λ_i	$\Delta\lambda_s$	R_c/P_0 [Mcps/mW]	$dR_c/d\lambda/P_0$ [Mcps/mW/nm]	η_s	η_i
Type-0	784 nm, 839 nm	~2.3 nm	1	0.46	0.45	0.35
Type-II[a]	810 nm, 810 nm	~0.3 nm	0.008	0.026	0.45	0.39

[a]Spectral interference filters centered at 810 nm (FWHM ~ 3 nm) were inserted to reduce detected singles coming from fluorescence.

(d_{zzz}^2/d_{yyz}^2) [27,28]. Spectral brightness was almost independent of wavelength degeneracy and bandwidth, except for the type-0 process and at temperatures below the wavelength-degeneracy point (since the type-0 collinear QPM condition is no longer met). The total pair rate of the type-0 crystal, however, peaked close to the degeneracy point and was two orders of magnitude higher than that of the type-II sample, due to the larger bandwidth.

The coincidence-to-single ratios obtained (Table 1) for both configurations are among the highest values demonstrated for photon-pair sources using Si-SPADs [6,11,13,14]. Note that these values were obtained without correction for detector inefficiencies or dark counts. Correspondingly, the maximum achievable heralding efficiency is that of the Si-SPAD itself, ~50% (higher uncorrected heralding efficiencies are achievable using transition edge sensors [10]). The experimental heralding efficiency was decreased further by other sources of loss, such as imperfect splitting ratio of the PBS and dichroic mirror, transmittance of the optical filters, and coupling of the spatially multimode SPDC emission into the single-mode fiber. The latter source of loss was minimized by our choice of focus geometry. We determined the loss due to single-mode fiber coupling to be less than 10%, by comparing the heralding efficiencies achieved with the Nufern HP780 single-mode fibers used in the experiment and multimode fibers.

C. Multimode cw-Pumped SPDC

The suitability of employing multimode FR cw pump laser diodes (FWHM bandwidth ~1 nm) for SPDC has not yet been investigated extensively, since single-mode lasers (FWHM < 500 MHz) are readily available in most quantum optics laboratories. However, for applications involving long propagation distances in harsh environments, such as space [21–24], the increased compactness, relaxed stabilization requirements, as well as high pump powers, could make FR laser diode-pumped SPDC a very attractive option. In order to evaluate the feasibility of using FR laser diode pumps for applications in quantum communication and cryptography, we analyzed the impact on the spectral properties and efficiency of the SPDC process.

The frequency modes of the FR laser diode have no fixed phase relationship, and consequently, the total resulting SPDC spectrum of the signal (idler) photons, $S(\lambda_{s(i)})$, is obtained by summing over the spectral intensity distributions, $S_\nu(\lambda_{s(i)})$, of all longitudinal pump modes: $S(\lambda_{s(i)}) = \sum_\nu I_\nu S_\nu(\lambda_{s(i)})$, where I_ν is the weight of the ν th pump mode in the pump spectrum $s(\lambda_p) \sim \sum_\nu I_\nu \delta(\lambda_p - \lambda_p^\nu)$. This leads to qualitative characteristics such as those depicted in Fig. 4, where we have calculated the spectra for type-0 and type-II QPM in KTP with a cw pump consisting of four longitudinal modes. A closer look at Fig. 4 shows that the spacing of the cwls of the downconverted signal (idler) photons generated by neighboring pump modes $(\lambda_{s(i)}^{\nu+1} - \lambda_{s(i)}^\nu)$ is increased with respect to the initial spectral mode spacing of the pump photons $(\lambda_p^{\nu+1} - \lambda_p^\nu)$. The effective multiplication factors $(M_{s(i)})$ that map the spacing of the pump modes to that of the generated cwls of the signal (idler) photons,

$$M_{s(i)}\left(\lambda_p^{\nu+1} - \lambda_p^\nu\right) \approx \left(\lambda_{s(i)}^{\nu+1} - \lambda_{s(i)}^\nu\right), \tag{1}$$

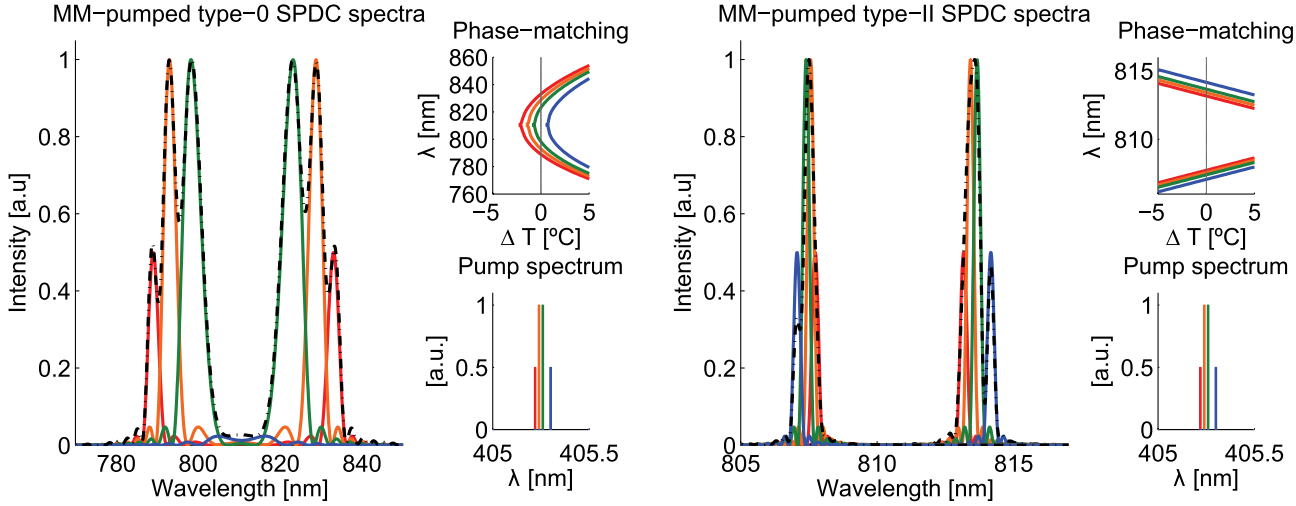

Fig. 4. Qualitative explanation of type-0 (left) and type-II (right) SPDC spectra with a multimode pump: at the reference temperature $\Delta T = 0$, multiple spectral modes of the pump are phase-matched at different cwls, resulting in a broadband SPDC response (dashed envelope). For the type-0 SPDC process depicted, the longest wavelength of the pump is not phase-matched. This is contrasted by the type-II process, in which all pump components contribute to the SPDC signal observed. Nevertheless, due to the QPM characteristics of type-II SPDC in ppKTP, the resulting SPDC bandwidth is still significantly smaller than that of the type-0 process.

vary depending on the QPM configuration and wavelengths. For KTP and the wavelengths under consideration, the multiplication factors are significantly larger for type-0 QPM ($M_s^0 \sim 124$ and $M_i^0 \sim 148$) than for type-II QPM ($M_s^{\mathrm{II}} \sim 8$ and $M_i^{\mathrm{II}} \sim 12$). Correspondingly, in addition to the spectral bandwidth of individual modes being larger (see Fig. 2), the larger multiplication factor leads to a significantly increased spectral bandwidth for type-0 SPDC. At this point, it is also interesting to note the potential application of this feature in metrology, since it allows inferring the pump spectrum with high resolution, by measurement of the signal and idler with a low-resolution spectrometer [43]. In conclusion, this brief analysis illustrates how the spectral properties in multifrequency-pumped SPDC depend strongly on the phase-matching temperature and pump spectrum, in particular, for type-0 SPDC.

In addition to the spectral characteristics, the total flux of the photon pairs generated is also affected when using a FR laser diode. The rate of photon pair generation by the υth pump mode is proportional to the respective downconversion bandwidth ($R_c^\nu \propto I^\nu \Delta\lambda_s^\nu$), which can vary strongly over the pump bandwidth, in particular, for type-0 SPDC. In this case, the total pair rate $R_c \propto \sum_\nu I^\nu \Delta\lambda_s^\nu$ can differ significantly from that achieved with a single-frequency pump of the same total power $I = \sum_\nu I_\nu$. For type-II SPDC with typical FR laser diode bandwidths of ~1 nm, the downconversion bandwidth remains almost constant for the different pump modes, and the total pair rates can be expected to be of similar magnitude as when using a single-mode pump.

In order to corroborate these theoretical findings, we experimentally compared the spectral properties and efficiencies of single-mode and multimode pumping. For the experimental comparison to take place under otherwise equal conditions, we achieved multimode and single-mode operation by detuning the temperature of the same laser diode. The resulting pump spectra were monitored using a high-resolution optical spectrum analyzer (inset in Fig. 5), and the SPDC spectra were measured using a diffraction-grating-based tunable filter (FWHM bandpass 0.4 nm). The experimental setup for the comparison of multimode- and single-mode-pumped SPDC was modified with respect to the previous section; the results were obtained with 11.5-mm (type-0) and 15-mm (type-II) ppKTP samples, and signal and idler photons were separated using an in-fiber beam splitter, without affecting any of the main conclusions of the analysis.

The experimental observations were in good agreement with the qualitative analysis in the previous paragraph. Two examples of multimode-pumped SPDC spectra are depicted alongside the single-mode-pumped spectrum as a reference in Fig. 5. Figure 5 also includes the SPDC spectra calculated for the multimode pump profiles, which were measured with the optical spectrum analyzer. The peaks resulting from the pump's most pronounced spectral modes can be identified in the spectra of both type-0 and type-II SPDC. Note that for the spectra calculated to better overlap with the experiment, we used poling periods that slightly deviated from the manufacturer's specifications. The difference in the relative weights of the calculated and experimental SPDC peaks is the result of wavelength-dependent losses, due to chromatic aberrations in the single-mode collection optics and the wavelength dependence of the spectrometer.

The pair rates measured for type-0 SPDC with a multimode pump were significantly lower than those measured with the single-mode pump, even when the temperature was chosen to phase match the entire pump bandwidth. This difference in efficiency was in part due to the aforementioned chromatic aberrations in the single-mode collection optics. Additionally, for type-0 SPDC, the short-wavelength spectral components of the pump lead to a smaller downconverted bandwidth (due to the larger nondegeneracy of the generated signal and idler for a fixed crystal temperature) and thus, contribute less pairs to the total broadband SPDC signal, as outlined in the previous paragraph. In addition to the decreased efficiency, another point of practical interest is the achievable entanglement visibility. Since the SPDC spectrum is distributed over a

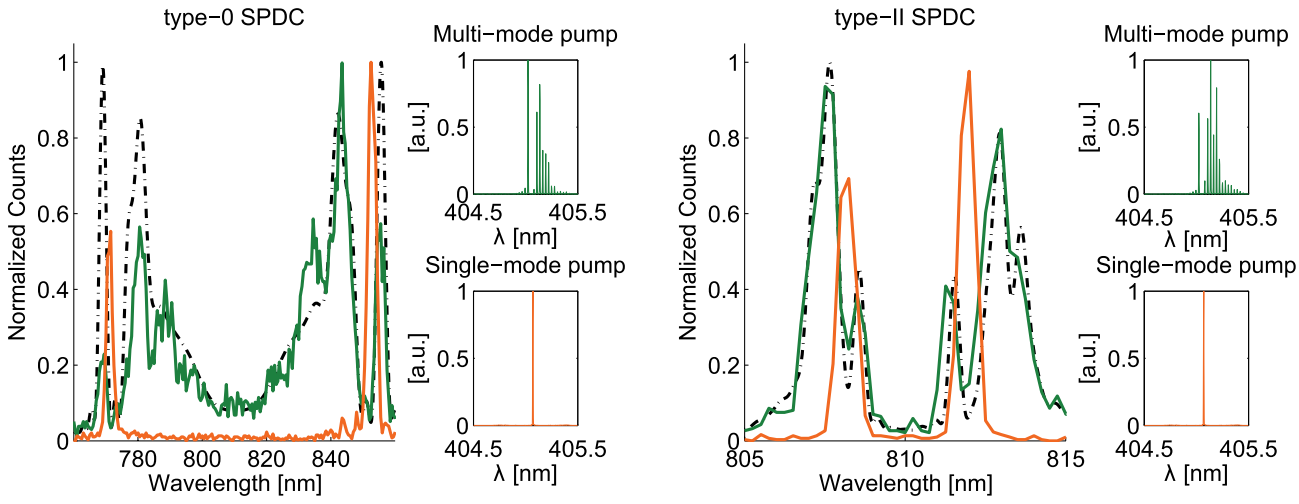

Fig. 5. Normalized SPDC spectra with multifrequency (experiment, green; theory, dashed black) and single-frequency pumps (experiment, orange) for type-0 (type-II) QPM in 11 mm (15 mm) of ppKTP. The differences between theory and experiment are the result of wavelength-dependent loss in the single-mode collection optics and spectrometer. For a multifrequency pump, the type-0 SPDC spectrum (left) covers a spectral range that is too broad for many applications, and would require strong spectral filtering. The type-II SPDC spectrum (right) is relatively robust with respect to the large pump bandwidth and could still be a feasible option for, e.g., free-space quantum communications and other standard quantum optics applications.

very large spectral range for the type-0 ppKTP crystal, polarization mode dispersion could make it difficult to achieve high-visibility polarization entanglement.

Notwithstanding, type-II SPDC did not show such a strong change in efficiency and spectral properties.

In conclusion, we thus believe that a type-II phase-matched crystal pumped with a high-power FR laser diode could provide a more robust choice for applications in out-of-the-lab operating conditions. High-visibility polarization entanglement using FR laser diodes has been demonstrated for beta-barium borate in [14], and we expect that these results can be extended to ppKTP. The criticality of required compensation techniques, as well as the suitability of various entanglement schemes (crossed-crystal [44], double-pass [8], Sagnac-loop [19]), for the case of FR laser diode-pumped ppKTP is to be assessed in further studies. Our results on spectral characteristics are complemented by the investigation of the coherence properties of multimode cw-pumped SPDC [45] and could be of great interest for applications in (quantum) metrology.

3. POLARIZATION ENTANGLEMENT IN A SAGNAC INTERFEROMETER

We generate polarization entanglement in a Sagnac interferometer [19] since this configuration is particularly well suited for simultaneously achieving high brightness and heralding efficiency. In contrast to other schemes, such as the sandwiched crystal scheme [7,44] (in which the pump waist is located at the center interface of two crossed crystals), the symmetric geometry of the interferometer allows the beam waists of the pump and collection optics to be focused at the center of the nonlinear crystal. This optimizes the spatial overlap of SPDC emission and the fiber-matched collection modes, which is particularly important when using long periodically poled nonlinear crystals. Achieving a perfectly symmetric Sagnac loop in practice is challenging; both the clockwise and counter-clockwise propagation modes must overlap with the spatial modes of the collection optics and all beam waists should be located at the crystal center [46]. Our choice of large beam waists somewhat relaxes the alignment tolerances, thus allowing high heralding efficiencies with standard off-the-shelf optomechanics.

Another advantage of the Sagnac scheme is that the autocompensating nature of the configuration allowed us to switch between operation in nondegenerate type-0 [20] and type-II QPM [6] configurations without adding specifically tailored walk-off compensation crystals, as required, for instance, in sandwiched crystal [44] or folded sandwich [8] configurations.

A. Experimental Setup

In the experimental setup (Fig. 6), a 405-nm grating-stabilized single-frequency laser diode was coupled into a single-mode fiber and focused to a beam waist of $w_p \sim 150$ μm at the center of a 20-mm-long type-0 or type-II ppKTP crystal. The crystals were mounted side-by-side on a temperature controller (TEC) and could be exchanged using a translation stage. For the type-0 crystal, the temperature was set to 30°C, phase-matching a collinear nondegenerate type-0 SPDC process with cwls of ~784 nm (signal) and ~839 nm (idler). For the type-II

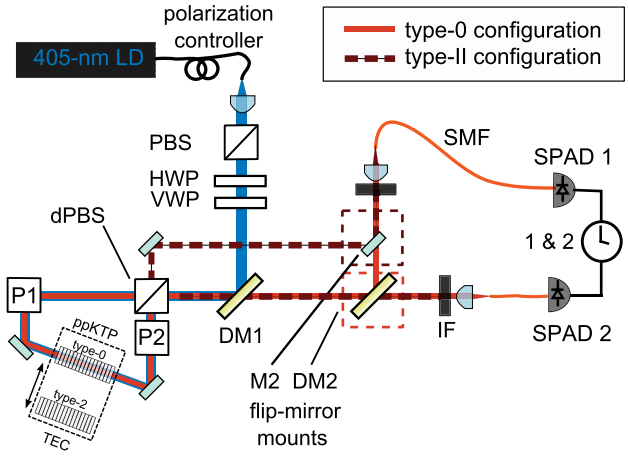

Fig. 6. Schematic setup of the Sagnac interferometer: a 405-nm cw laser diode, with its polarization state set by a combination of a PBS, a HWP, and a VWP, is focused to the center of one of two ppKTP crystals (type-0/II), placed at the center of the Sagnac loop. The Sagnac interferometer consists of a dPBS, two periscopes (P1, P2), and broadband high-reflection-coated mirrors. The downconverted photons traverse interference filters (IF) and are coupled into single-mode fibers (SMF). A dichroic mirror (DM2) and a mirror (M2), mounted on flip-mirror mounts, allow switching between type-0 and type-II configurations.

sample, the temperature was set to 35°C, to phase-match a degenerate type-II SPDC process around 810 nm.

The crystals were placed at the center of a Sagnac interferometer, which consisted of a dual-wavelength PBS (dPBS—antireflection-coated at 810 and 405 nm), two periscopes (P1, P2), and two additional beam-steering mirrors (broadband, highly reflective). In one arm of the interferometer, polarization was flipped using a cross-faced periscope (P1), while a parallel-faced periscope (P2) displaced photons propagating in the other arm to the same height, while leaving the polarization state unchanged [20,47]. This way the pump beam enters the crystal along the phase-matched axis for both propagation directions. Furthermore, the polarization flip ensures temporal indistinguishability between the signal and idler photons after the dPBS, which arises due to birefringent (type-II) and dispersive (type-0) walk-off in the ppKTP crystal.

With either sample placed in the pump beam, the SPDC generated in the nonlinear crystal was isolated from the pump photons via a highly reflective dichroic mirror (DM1) and was coupled into a Nufern HP780 single-mode fiber, using an $f = 18.4$ mm aspheric lens. Note that in the type-II configuration, signal and idler photons exit through distinct exit ports of the dPBS, whereas for type-0 SPDC from both propagation modes is emitted back into the pump mode. Consequently, in the type-0 configuration, the signal and idler were split using an additional dichroic mirror (DM2) with its transition edge at 810 nm located after DM1. The dichroic mirror (DM2) and a beam-steering mirror (M2) were mounted on flip-mirror mounts, to facilitate switching between the two modes of operation (Typically, a few minutes were required for re-alignment.) If the relative magnitudes of the horizontally and vertically polarized pump components are set accordingly, photon pairs are equally likely to be generated in either clockwise or counter-clockwise emission mode and a polarization-entangled state of the form $|\Phi(\phi)\rangle = 1/\sqrt{2}(|V_{\lambda_s} V_{\lambda_i}\rangle + e^{i\phi}|H_{\lambda_s} H_{\lambda_i}\rangle)$ or $|\Psi(\phi)\rangle = 1/\sqrt{2}(|V_{\lambda_s} H_{\lambda_i}\rangle + e^{i\phi}|H_{\lambda_s} V_{\lambda_i}\rangle)$, respectively, results for type-0 and type-II QPM. Equal

Table 2. Low-Flux Performance Characteristics of the Entangled Photon Source for Type-0 and Type-II QPM in a Bidirectionally Pumped Configuration

Configuration[a]	$\Delta\lambda_s$	R_c/P_0 [Mcps/mW]	$dR_c/d\lambda/P_0$ [Mcps/mW/nm]	η_s	η_i	Fidelity[b]
Nondegenerate type-0[c]	∼2.3 nm	0.5	0.22	0.31	0.31	$99.1 \pm 0.2\%$
Degenerate type-II	∼0.3 nm	0.007	0.02	0.40	0.37	$99.4 \pm 0.2\%$

[a]Polarizers removed from the setup for efficiency measurements.
[b]Thin-film polarizers and achromatic quarter-wave plates were inserted for fidelity measurement.
[c]Compared with the configuration used in Table 1, an interference filter centered at 785 nm (3.5 nm FWHM) was added to the signal arm.

pair-emission probabilities were ensured by setting the polarization of the incoming pump beam to balance the respective coincidence rates via a half-wave plate (HWP). The relative phase of the entangled state, ϕ, was then set by tilting a variable wave plate (VWP) consisting of 100 μm of YVO_4 about its optical axis.

B. Experimental Performance

We identified twofold pair-detection events via two fiber-coupled SPADs and a fast electronic AND gate with a coincidence window set to ∼4.5 ns. To assess the quality of the entangled state, we measured the Bell-state fidelity via the fidelity witnesses $F = \langle\Phi^{\pm}|\rho|\Phi^{\pm}\rangle = (1 + V_{H/V} \pm V_{D/A} \mp V_{L/R})/4$ and $F = \langle\Psi^{\pm}|\rho|\Psi^{\pm}\rangle = (1 + V_{H/V} \pm V_{D/A} \pm V_{L/R})/4$ [48], where $V_{ij} = (N_{ii} + N_{jj} - N_{ij} - N_{ji})/(N_{ii} + N_{jj} + N_{ij} + N_{ji})$ are the visibilities in three mutually unbiased measurement bases (here $ij = H/V, L/R, D/A$) and N_{ij} are the detected coincidence counts. For both ppKTP samples, fidelity was assessed at low flux rates, such that the impact of accidental coincidences on fidelity was negligible [8–10].

C. Type-II QPM Configuration

For a pump power of 1.7 mW incident on the type-II crystal, we observed a spectrally broadband fluorescent singles background. In order to obtain a high heralding efficiency, interference filters centered at 810 nm with a 3 nm FWHM passband (significantly larger than the SPDC bandwidth of ∼0.3 nm) were inserted into the paths of both signal and idler photons. With the filters in place, we detected a coincidence rate of $R_c = 12.4$ kcps and singles rates of $R_s = 34$ kcps and $R_i = 31$ kcps, corresponding to a detected pair rate of 0.007 Mcps/mW and a detected spectral brightness of 0.02 Mcps/mW/nm. Without correcting for background counts, losses, or detection inefficiency, we measure an overall signal (idler) heralding efficiency of $\eta_s = R_c/R_i = 0.40$ ($\eta_i = R_c/R_s = 0.37$). Note that the heralding efficiencies achieved while pumping the Sagnac loop bidirectionally (Table 2) were approximately 10% lower than when pumping only in the clockwise direction (Table 1), due to imperfect alignment of the clockwise and counter-clockwise propagation modes.

The high degree of polarization entanglement was confirmed at low flux rates, where we measured visibilities of $V_{H/V} = 99.7 \pm 0.1\%$, $V_{D/A} = 98.9 \pm 0.2\%$, and $V_{L/R} = 98.9 \pm 0.2\%$, corresponding to $F = 99.4 \pm 0.2\%$.

D. Type-0 QPM Configuration

Operating in a type-0 QPM configuration, the source is capable of significantly higher pair rates. However, owing to the larger spectral bandwidth, the clockwise and counter-clockwise SPDC emission acquired slightly different phase characteristics over the entire bandwidth (group velocity distribution in the mirrors and dPBS). A high degree of polarization entanglement could still be achieved, by placing an interference filter (FWHM ∼ 3.5 nm) and a thin birefringent compensation crystal (100-μm yttrium vanadate) in the signal path. At low flux rates, we obtain $V_{H/V} = 99.7 \pm 0.1\%$, $V_{D/A} = 98.3 \pm 0.2\%$, and $V_{L/R} = 98.4 \pm 0.2\%$, which corresponds to $F = 99.1 \pm 0.2\%$.

With the polarizes removed from the setup, we detected a coincidence rate of $R_c = 19$ kcps and singles rates of $R_s = 63$ kcps and $R_i = 62$ kcps, pump power of 0.03 mW, which corresponds to a normalized detected pair rate of 0.5 Mcps/mW and a detected spectral brightness of 0.22 Mcps/mW/nm.

Heralding efficiency was lower in the type-0 configuration, since the dPBS was specifically designed for 810 and 405 nm, and not for triple-wavelength operation required for nondegenerate type-0 SPDC. The limited extinction of the dPBS resulted in a slightly higher loss and, correspondingly, a lower heralding efficiency (see Table 2).

4. CONCLUSION

We have demonstrated a bright, high-heralding-efficiency source of polarization-entangled photons based on SPDC from a single 20-mm ppKTP crystal in a Sagnac interferometer. We compared type-II and type-0 QPM configurations in terms of efficiency, as well as temperature- and pump wavelength-dependent spectral properties.

As expected from the different nonlinear coefficients, type-0 SPDC in ppKTP was significantly more efficient than type-II, allowing both high brightness and heralding efficiency for moderate pump powers. However, type-II QPM in ppKTP is more robust with respect to temperature drifts. Furthermore, type-II QPM is less affected by larger pump bandwidths and allows generating comparatively narrow SPDC bandwidths, even when pumping with a FR cw laser diode. The use of a FR pump is particularly attractive, due to relaxed requirements in terms of current and temperature stabilization, compactness, and the generally higher powers compared with cw operation.

These results can be of great practical interest to experimenters developing ultrabright, compact, and robust sources with high heralding efficiency, as required for applications in quantum metrology and quantum information, and their implementation in harsh environmental conditions, such as those in space [21–24].

ACKNOWLEDGMENTS

The authors thank Sven Ramelow for discussions and advice on the source design, and Daniel Perez for support in programming the data acquisition software. We also thank two anonymous reviewers for constructive criticism and suggestions that contributed to the final version of the paper. FS acknowledges the financial support via the FPI fellowship

of the Spanish Ministry of Science and Innovation (MICINN). This work was made possible by grants from the European Space Agency (contracts 21460/08/NL/IA, 22542/09/NL/SFe, and 4000104180/11/NL/AF); the Austrian FFG for the QTS project (No. 828316) within the ASAP 7 program; and the Spanish MICINN via contracts TEC2010-14832, FIS2011-23520, and FIS2010-14831. We also acknowledge support by the European Commission, grant Q-ESSENCE (No. 248095).

REFERENCES

1. W. Tittel and G. Weihs, "Photonic entanglement for fundamental tests and quantum communication," Quantum Inf. Comput. **1**, 3–56 (2001).
2. J. L. O'Brien, A. Furusawa, and J. Vucovic, "Photonic quantum technologies," Nat. Photonics **3**, 687–695 (2009).
3. P. Michler, A. Kiraz, C. Becher, W. V. Schoenfeld, P. M. Petroff, L. Zhang, E. Hu, and A. Imamoglu, "A quantum dot single-photon turnstile device," Science **290**, 2282–2285 (2000).
4. J. Fulconis, O. Alibart, J. L. O'Brien, W. J. Wadsworth, and J. G. Rarity, "Nonclassical interference and entanglement generation using a photonic crystal fiber pair photon source," Phys. Rev. Lett. **99**, 120501 (2007).
5. M. Medic, J. B. Altepeter, M. A. Hall, M. Patel, and P. Kumar, "Fiber-based telecommunication-band source of degenerate entangled photons," Opt. Lett. **35**, 802–804 (2010).
6. A. Fedrizzi, T. Herbst, A. Poppe, T. Jennewein, and A. Zeilinger, "A wavelength-tunable fiber-coupled source of narrowband entangled photons," Opt. Express **15**, 15377–15386 (2007).
7. F. Steinlechner, P. Trojek, M. Jofre, H. Weier, D. Perez, T. Jennewein, R. Ursin, J. Rarity, M. W. Mitchell, J. P. Torres, H. Weinfurter, and V. Pruneri, "A high-brightness source of polarization-entangled photons optimized for applications in free space," Opt. Express **20**, 9640–9649 (2012).
8. F. Steinlechner, S. Ramelow, M. Jofre, M. Gilaberte, T. Jennewein, J. P. Torres, M. W. Mitchell, and V. Pruneri, "Phase-stable source of polarization-entangled photons in a linear double-pass configuration," Opt. Express **21**, 11943–11951 (2013).
9. H. Takesue and K. Shimizu, "Effects of multiple pairs on visibility measurements of entangled photons generated by spontaneous parametric processes," Opt. Commun. **283**, 276–287 (2010).
10. S. Ramelow, A. Mech, M. Giustina, S. Gröblacher, W. Wieczorek, J. Beyer, A. Lita, B. Calkins, T. Gerrits, S. W. Nam, A. Zeilinger, and R. Ursin, "Highly efficient heralding of entangled single photons," Opt. Express **21**, 6707–6717 (2013).
11. M. D. C. Pereira, F. E. Becerra, B. L. Glebov, J. Fan, S. W. Nam, and A. Migdall, "Demonstrating highly symmetric single-mode, single-photon heralding efficiency in spontaneous parametric downconversion," Opt. Lett. **38**, 1609–1611 (2013).
12. S. Krapick, H. Herrmann, V. Quiring, B. Brecht, H. Suche, and C. Silberhorn, "An efficient integrated two-color source for heralded single photons," New J. Phys. **15**, 033010 (2013).
13. C. Söller, O. Cohen, B. J. Smith, I. A. Walmsley, and C. Silberhorn, "High-performance single-photon generation with commercial-grade optical fiber," Phys. Rev. A **83**, 031806 (2011).
14. P. Trojek and H. Weinfurter, "Collinear source of polarization-entangled photon pairs at nondegenerate wavelengths," Appl. Phys. Lett. **92**, 211103 (2008).
15. M. Giustina, A. Mech, S. Ramelow, B. Wittmann, J. Kofler, J. Beyer, A. Lita, B. Calkins, T. Gerrits, S. W. Nam, R. Ursin, and A. Zeilinger, "Bell violation using entangled photons without the fair-sampling assumption," Nature **497**, 227–230 (2013).
16. B. Wittmann, S. Ramelow, F. Steinlechner, N. K. Langford, N. Brunner, H. M. Wiseman, R. Ursin, and A. Zeilinger, "Loophole-free Einstein–Podolsky–Rosen experiment via quantum steering," New J. Phys. **14**, 053030 (2012).
17. B. G. Christensen, K. T. McCusker, J. B. Altepeter, B. Calkins, T. Gerrits, A. E. Lita, A. Miller, L. K. Shalm, Y. Zhang, S. W. Nam, N. Brunner, C. C. W. Lim, N. Gisin, and P. G. Kwiat, "Detection-loophole-free test of quantum nonlocality, and applications," Phys. Rev. Lett. **111**, 130406 (2013).
18. B.-S. Shi and A. Tomita, "Generation of a pulsed polarization entangled photon pair using a Sagnac interferometer," Phys. Rev. A **69**, 013803 (2004).
19. T. Kim, M. Fiorentino, and F. N. C. Wong, "Phase-stable source of polarization-entangled photons using a polarization Sagnac interferometer," Phys. Rev. A **73**, 012316 (2006).
20. M. Hentschel, H. Hübel, A. Poppe, and A. Zeilinger, "Three-color Sagnac source of polarization-entangled photon pairs," Opt. Express **17**, 23153–23159 (2009).
21. J. G. Rarity, P. R. Tapster, P. M. Gorman, and P. Knight, "Ground to satellite secure key exchange using quantum cryptography," New J. Phys. **4**, 82 (2002).
22. C. Bonato, A. Tomaello, V. D. Deppo, G. Naletto, and P. Villoresi, "Feasibility of satellite quantum key distribution," New J. Phys. **11**, 045017 (2009).
23. T. Scheidl, E. Wille, and R. Ursin, "Quantum optics experiments using the international space station: a proposal," New J. Phys. **15**, 043008 (2013).
24. D. Rideout, T. Jennewein, G. Amelino-Camelia, T. F. Demarie, B. L. Higgins, A. Kempf, A. Kent, R. Laflamme, X. Ma, R. B. Mann, E. Martín-Martínez, N. C. Menicucci, J. Moffat, C. Simon, R. Sorkin, L. Smolin, and D. R. Terno, "Fundamental quantum optics experiments conceivable with satellites—reaching relativistic distances and velocities," Classical Quantum Gravity **29**, 224011 (2012).
25. R. Ursin, T. Jennewein, J. Kofler, J. M. Perdigues, L. Cacciapuoti, C. J. de Matos, M. Aspelmeyer, A. Valencia, T. Scheidl, A. Acin, C. Barbieri, G. Bianco, C. Brukner, J. Capmany, S. Cova, D. Giggenbach, W. Leeb, R. H. Hadfield, R. Laflamme, N. Lütkenhaus, G. Milburn, M. Peev, T. Ralph, J. Rarity, R. Renner, E. Samain, N. Solomos, W. Tittel, J. P. Torres, M. Toyoshima, A. Ortigosa-Blanch, V. Pruneri, P. Villoresi, I. Walmsley, G. Weihs, H. Weinfurter, M. Zukowski, and A. Zeilinger, "Space-quest, experiments with quantum entanglement in space," Europhy. News **40**, 26–29 (2009).
26. M. N. Satyanarayan, A. Deepthy, and H. L. Bhat, "Potassium titanyl phosphate and its isomorphs: growth, properties, and applications," Crit. Rev. Solid State Mater. Sci. **24**, 103–191 (1999).
27. H. Vanherzeele and J. D. Bierlein, "Magnitude of the nonlinear-optical coefficients of $KTiOPO_4$," Opt. Lett. **17**, 982–984 (1992).
28. M. V. Pack, D. J. Armstrong, and A. V. Smith, "Measurement of the $\chi(2)$ tensors of $KTiOPO_4$, $KTiOAsO_4$, $RbTiOPO_4$, and $RbTiOAsO_4$ crystals," Appl. Opt. **43**, 3319–3323 (2004).
29. R. Boyd, *Nonlinear Optics* (Academic, 2003).
30. B. E. A. Saleh and M. C. Teich, *Nonlinear Optics* (Wiley, 2001), pp. 737–798.
31. S. Lerch, B. Bessire, C. Bernhard, T. Feurer, and A. Stefanov, "Tuning curve of type-0 spontaneous parametric down-conversion," J. Opt. Soc. Am. B **30**, 953–958 (2013).
32. S.-Y. Baek and Y.-H. Kim, "Spectral properties of entangled photons generated via type-I frequency-nondegenerate spontaneous parametric down-conversion," Phys. Rev. A **80**, 033814 (2009).
33. W. P. Grice and I. A. Walmsley, "Spectral information and distinguishability in type-II down-conversion with a broadband pump," Phys. Rev. A **56**, 1627–1634 (1997).
34. Y.-H. Kim and W. P. Grice, "Measurement of the spectral properties of the two-photon state generated via type II spontaneous parametric downconversion," Opt. Lett. **30**, 908–910 (2005).
35. B. Dayan, A. Pe'er, A. A. Friesem, and Y. Silberberg, "Nonlinear interactions with an ultrahigh flux of broadband entangled photons," Phys. Rev. Lett. **94**, 043602 (2005).
36. M. B. Nasr, S. Carrasco, B. E. A. Saleh, A. V. Sergienko, M. C. Teich, J. P. Torres, L. Torner, D. S. Hum, and M. M. Fejer, "Ultrabroadband biphotons generated via chirped quasi-phase-matched optical parametric down-conversion," Phys. Rev. Lett. **100**, 183601 (2008).
37. T. Y. Fan, C. E. Huang, B. Q. Hu, R. C. Eckardt, Y. X. Fan, R. L. Byer, and R. S. Feigelson, "Second harmonic generation and accurate index of refraction measurements in flux-grown $KTiOPO_4$," Appl. Opt. **26**, 2390–2394 (1987).
38. W. Wiechmann, S. Kubota, T. Fukui, and H. Masuda, "Refractive-index temperature derivatives of potassium titanyl phosphate," Opt. Lett. **18**, 1208–1210 (1993).

39. R. S. Bennink, "Optimal collinear Gaussian beams for spontaneous parametric down-conversion," Phys. Rev. A **81**, 053805 (2010).
40. D. Ljunggren and M. Tengner, "Optimal focusing for maximal collection of entangled narrow-band photon pairs into single-mode fibers," Phys. Rev. A **72**, 062301 (2005).
41. T. Guerreiro, A. Martin, B. Sanguinetti, N. Bruno, H. Zbinden, and R. T. Thew, "High efficiency coupling of photon pairs in practice," Opt. Express **21**, 27641–27651 (2013).
42. G. D. Boyd and D. A. Kleinman, "Parametric interaction of focused Gaussian light beams," J. Appl. Phys. **39**, 3597–3639 (1968).
43. S. Ramelow and R. Lapkiewicz, private communication (2013).
44. P. G. Kwiat, E. Waks, A. G. White, I. Appelbaum, and P. H. Eberhard, "Ultrabright source of polarization-entangled photons," Phys. Rev. A **60**, R773–R776 (1999).
45. O. Kwon, Y.-S. Ra, and Y.-H. Kim, "Coherence properties of spontaneous parametric down-conversion pumped by a multimode cw diode laser," Opt. Express **17**, 13059–13069 (2009).
46. A. Predojević, S. Grabher, and G. Weihs, "Pulsed Sagnac source of polarization entangled photon pairs," Opt. Express **20**, 25022–25029 (2012).
47. A. Arora and S. Ghosh, "A twisted periscope arrangement for transporting elliptically polarized light without change in its polarization state," Rev. Sci. Instrum. **81**, 123102 (2010).
48. O. Gühne and G. Toth, "Entanglement detection," Phys. Rep. **474**, 1–75 (2009).